Dual light field and polarization imaging using CMOS diffractive image sensors

Suren Jayasuriya,* Sriram Sivaramakrishnan, Ellen Chuang, Debashree Guruaribam, Albert Wang, and Alyosha Molnar

School of Electrical and Computer Engineering, Cornell University, Ithaca, New York 14853, USA
**Corresponding author: sj498@cornell.edu*

Received March 17, 2015; revised April 29, 2015; accepted April 30, 2015;
posted April 30, 2015 (Doc. ID 236226); published May 15, 2015

In this Letter we present, to the best of our knowledge, the first integrated CMOS image sensor that can simultaneously perform light field and polarization imaging without the use of external filters or additional optical elements. Previous work has shown how photodetectors with two stacks of integrated metal gratings above them (called angle sensitive pixels) diffract light in a Talbot pattern to capture four-dimensional light fields. We show, in addition to diffractive imaging, that these gratings polarize incoming light and characterize the response of these sensors to polarization and incidence angle. Finally, we show two applications of polarization imaging: imaging stress-induced birefringence and identifying specular reflections in scenes to improve light field algorithms for these scenes.

OCIS codes: (110.1758) Computational imaging; (230.5440) Polarization-selective devices; (110.5405) Polarimetric imaging; (040.1240) Arrays.
http://dx.doi.org/10.1364/OL.40.002433

Computational imaging has recently enabled new functionality and imaging modalities in the areas of three-dimensional photography and medical imaging, as well as computer graphics and vision [1]. In particular, the seminal paper on the light field by Levoy and Hanharan [2] heralded research on image-based rendering techniques where novel viewpoints of a scene can be rendered from the space of light rays in the scene. Applications of light field imaging include synthetic aperture refocusing to extend the depth of field, passive depth from defocus, and glare reduction [3,4]. Methods for capturing light fields have included camera arrays [5] and plenoptic cameras that place optical elements such as microlenses [6], transmission masks [7], or diffraction gratings in front of the sensor [8,9].

Another important imaging modality is polarization imaging that uses information about the polarization of incoming light. This information has been used for material identification [10], imaging through haze and fog [11], and enhancing biomedical endoscopy of cancerous tissue [12]. To detect polarization with image sensors, researchers have used pixelated polarization imaging cameras [13–16] or polarizing filters that tile the image sensor known as division of focal plane polarizers constructed from fabricated nanowires [17], aligned structures [18], or integrated metal interconnects [19]. Polarization has also been combined with three-dimensional imaging from digital holography in single-shot acquisition [20,21].

In this Letter, we present a CMOS image sensor with angle sensitive pixels (ASPs) that uses integrated diffractive metal gratings to simultaneously polarize incoming light and generate Talbot diffraction patterns that capture incident four-dimensional light fields. This image sensor is, to the best of our knowledge, the first of its kind to perform both types of imaging simultaneously without additional optical or mechanical components while integrated in an unmodified CMOS process. While previous work has explored ASPs for light field imaging [8,22], we extend the scope of these devices by characterizing their response to light polarization. We show applications of stress-induced birefringence imaging and tagging specular reflection which, combined with light field imaging, lead to new functionality and improved algorithms.

ASPs are photodetectors that use two stacks of diffraction gratings (50% duty cycle) designed in the CMOS metal interconnect layers [8]. Incident light impinging on the first grating forms a periodic diffraction pattern resembling the grating according to the Talbot effect with period $2d^2/\lambda$, where d is the pitch of the grating and λ is the wavelength. This pattern is filtered by a second grating set at a half-integer multiple of the Talbot depth and then sensed by photodiodes. The angular response of this pixel can be represented by the following expression [22]:

$$A(\boldsymbol{\theta}) * (1 + m\ \cos(\beta(\cos(\gamma)\theta_x + \sin(\gamma)\theta_y) + \alpha), \qquad (1)$$

where A is a Gaussian aperture function of incidence angle $\boldsymbol{\theta} = (\theta_x, \theta_y)$, m is the modulation efficiency of the pixel, β is the angular frequency related to the grating periodicity, γ is the grating orientation, and α is proportional to the offset of the second grating relative to the first grating. The Talbot effect has a wavelength dependence, so the gratings are designed for a 520 nm green light with minimal degradation of signal for other visible wavelengths [8]. As shown in Fig. 1, the image sensor, fabricated in an unmodified 180 nm CMOS process, is composed of a 6×4 tile of different ASPs whose diversity of angular responses in Eq. (1) can be used to recover the incidence angle of incoming light. Each pixel is 10 μm and the image sensor is composed of 64×96 tiles or correspondingly 384×384 pixels. From the angular response ASPs can resolve the direction of light rays and, thus, can recover a four-dimensional light field from a scene [22].

To extend the model to include polarization, we characterized the impulse response of the pixels by imaging a blurred out point source of light placed at optical infinity with a linear polarizing filter at different polarization

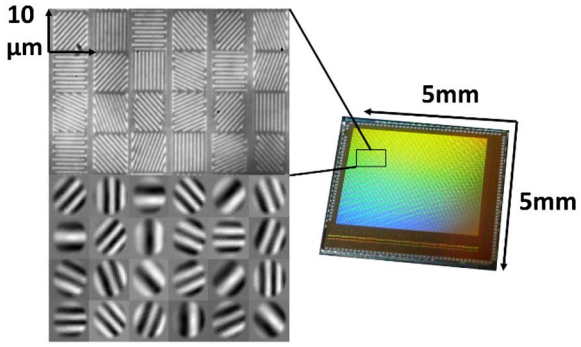

Fig. 1. Angle sensitive pixel (ASP) image sensor fabricated in 180 nm CMOS composed of 6×4 tile. The lower figure shows the corresponding two-dimensional angular point spread responses.

angles in front of the camera. The light source was a white LED emitting broadly across the visible spectrum which then passed through a diffuser and small pinhole to model a point source. The ASP sensor sees variation in the incidence angle across the blurred out spot as shown in Fig. 1. By adding the two sub-pixels with complementary phase separations ($\alpha = 0, 180$ or $90, 270$), we recover the common mode or average intensity at each pixel that shows a fixed aperture response for all pixel types [22]. Thus, any variation in the common mode between two pixels is because of that pixel's polarization response. The resolution of the polarization image is at the tile resolution of 64×96. Figure 2 shows that this intensity as a function of polarization has a response of $\cos(2(\psi - \gamma))$, where ψ is polarization angle and γ is the grating orientation. This conforms to the intuition that our diffraction gratings act similarly to wire grid polarizers. Therefore, the aperture function of the ASP response can be modulated by polarization as $\cos(2(\psi - \gamma))A(\boldsymbol{\theta})$. We note that the diffraction gratings act as primarily linear polarizers and, thus, extracting elliptical or circular polarization would require the use of waveplates not easily realized in CMOS structures.

We also characterized the polarization response with respect to grating orientation as shown in Fig. 3. From the 0, 45, 90, and 135 degree grating orientation ASPs, we can calculate the angle of polarization from their common mode responses to be

$$\psi = \tan^{-1}((I_{45} - I_{135})/(I_0 - I_{90})). \quad (2)$$

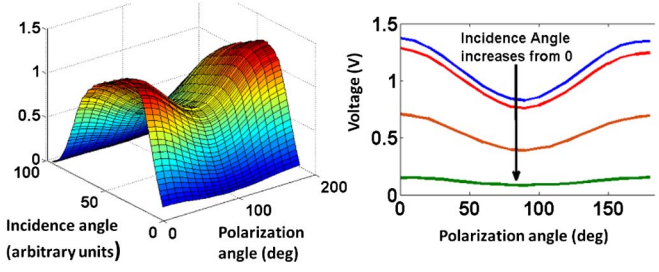

Fig. 2. Left figure plots common mode pixel output of polarization angle versus incidence angle in one-dimensional to show response $\cos(2(\psi - \gamma)) * e^{-\theta^2}$. Right plot shows cross section of this response at different incident angles.

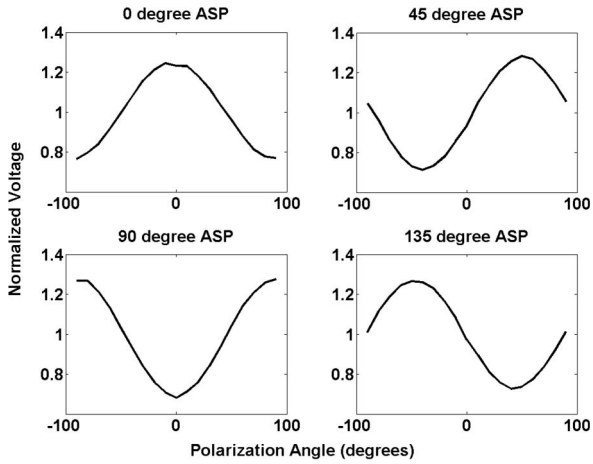

Fig. 3. Polarization response for ASPs with grating orientations of 0, 45, 90, and 135 degrees. Extinction ratios of approximately 2 were recorded.

We show a plot of the measured angle of polarization in Fig. 4. The degree of linear polarization was measured to be about 25%, and the average deviation between calculated and reference angles was 1.12 degrees. The extinction ratio was calculated to be around 2 which is somewhat lower than ratios for other CMOS polarizing sensors with integrated filters (~ ratio of 6-50 [17–19]). This is explained by the fact that the pitch of the gratings needs to be on the order of the wavelength of light to act as diffraction gratings (our pitch was 1 μm), and thus prohibits high extinction ratios obtained by wire grid polarizers with sub-wavelength structures [17]. This is a fundamental trade-off for any grating that wants to simultaneously polarize and diffract visible light.

In many transparent materials, stress induces birefringence in the material that changes the polarization of light passing through it. Detecting birefringence has several applications in biomedical microscopy, and ASP algorithms such as synthetic aperture refocusing can combine with detecting birefringence to increase the effectiveness of polarization microscopy. In Fig. 5, we show the results of stressing a sheet of clear polyethylene (thickness of 4 mil) with a force gauge while shining polarized light through the sheet. The force applied ranged up to 25 N, and reliable minimum detection could

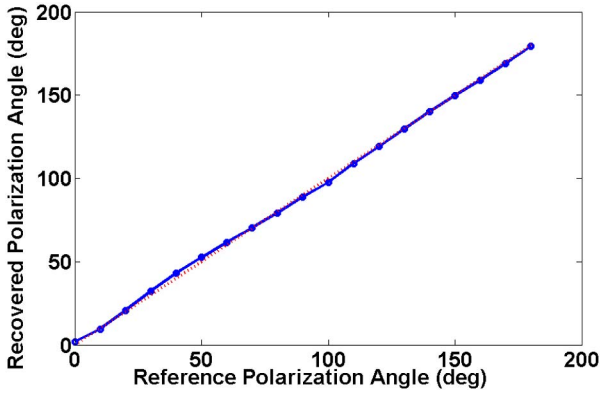

Fig. 4. Recovered polarization angle versus reference angle. The average deviation was around 1.12 degrees.

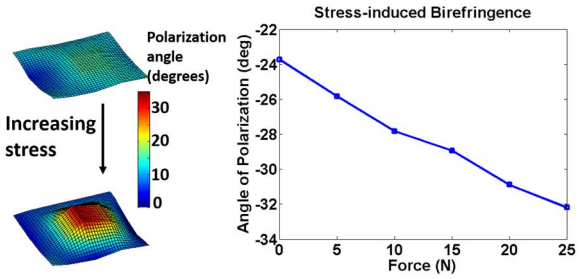

Fig. 5. Measuring change in polarization angle as a function of applied stress to polyethylene material. Minimum detectable force is 0.5 N.

be achieved for 0.5 N. Further detection is limited since the signal of interest is around 2–5 mV which is close to the noise of the image sensor.

Another important application of polarization imaging is to identify and remove specular reflection within scenes. Light undergoing refraction in dielectric materials reflects a polarized component that appears as a strong highlight. This specular reflection can lead to difficulty for computer vision and light field algorithms that make the modeling assumption of Lambertian surfaces with diffuse reflectance as shown in Fig. 6. Automatic tagging and reducing specular reflection using polarization can allow for better scene understanding and reconstruction in vision algorithms [23].

In Fig. 7, we show an image of a scene containing a pool ball with specular highlights and the image with specular reflections identified and tagged using the measured angle of polarization. We use differences in polarization images $I_0 - I_{90}$ and $I_{45} - I_{135}$ to detect specular reflection, and we use a threshold operation (around 30–40 mV) to avoid noise and low signal. One can note that the algorithms do not misidentify saturated pixels because of bright light as specular reflection, so the algorithm is robust even in those conditions. One main problem with using a tile of polarization sensors is that intensity variations across the tile because of edges can be mislabeled as changes in polarization. We reduce this effect in our image processing by selecting pixels close to one another for polarization calculations and correcting for the image gradient in a tile because of edges. We note that more advanced methods can be used as in [24].

In Fig. 8, we show a depth map computed from light field information captured by ASPs with a range of 1 m and depth precision of 2.5 mm [8]. Note that light field algorithms generally only estimate depth from edges in the scene. It is clear that the depth estimates fail on

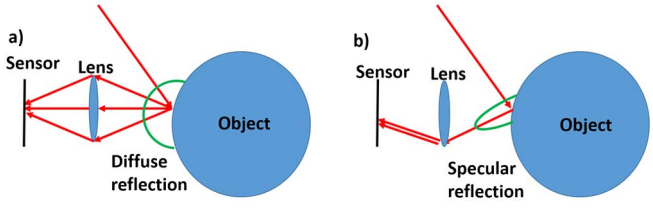

Fig. 6. (a) Diffuse reflection versus (b) specular reflection. Notice how the image sensor only receives rays from one specific angle in specular reflection which violates the Lambertian assumptions often made in computer vision algorithms.

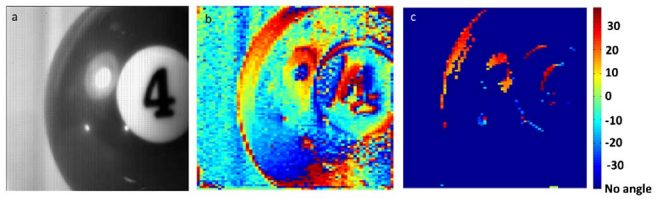

Fig. 7. (a) Scene with specular reflection, (b) the angle of polarization when no thresholding is performed, and (c) specular highlights tagged with a threshold of 40 mV.

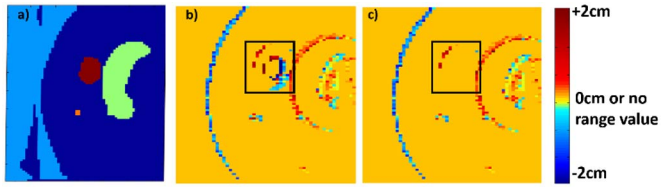

Fig. 8. (a) Image segmentation performed on the original image, (b) the depth map relative to the focal plane computed from light field captured by ASPs, and (c) the removal of inaccurate depths at the specular locations.

specular reflection. In Fig. 8, we show how using image segmentation and specular reflection tagging can remove these problem regions and lead to better depth accuracy of ASPs. We use image segmentation in the original image via thresholding and active contours, and then remove segments with a majority of pixels that are specular to remove specular highlights from the scene. This shows the advantage of dual light field and polarization imaging for specular reflection: the polarization information can enhance the performance and robustness of light field algorithms.

We have shown and characterized the polarization response of ASPs. There are interesting trade-offs between the design of gratings for good diffraction response (corresponding to the modulation efficiency) and the extinction ratio for polarization. Polarization can be modeled in light field imaging as an additional sinusoidal modulation multiplied to the pixel response. We showed the ability to image stress-induced birefringence using ASPs, and showed how automatic specular reflection tagging can improve traditional light field depth algorithms. Future applications include utilizing the lensless capabilities of ASPs with polarization for enhanced microscopy. We hope that the combination of light field and polarization imaging leads to new functionality and imaging modalities.

The authors would like to thank Steven Miller for helpful discussions regarding this work. S. J. was funded by an NSF Graduate Research Fellowship award DGE-1144153, and A. M. was funded by an NSF CAREER award no.1150329.

References

1. R. Raskar and J. Tumblin, *Computational Photography, Synthesis Lectures on Computer Graphics and Animation* (Morgan & Claypool, 2007).
2. M. Levoy and P. Hanrahan, *Proc. SIGGRAPH* (ACM, 1996), pp. 31–42.

3. A. Levin, R. Fergus, F. Durand, and W. T. Freeman, ACM Trans. Graphics **26**, 70 (2007).
4. R. Raskar, A. Agrawal, C. Wilson, and A. Veeraraghavan, ACM Trans. Graphics **27**, 1 (2008).
5. B. Wilburn, N. Joshi, V. Vaish, E. Talvala, E. Anutnez, A. Barth, A. Adams, M. Horowitz, and M. Levoy, ACM Trans. Graphics **24**, 765 (2005).
6. E. Adelson and J. Wang, IEEE Trans. Pattern Anal. Mach. Intell. **14**, 99 (1992).
7. A. Veeraraghavan, R. Raskar, A. Agrawal, A. Mohan, and J. Tumblin, ACM Trans. Graphics **26**, 69 (2007).
8. A. Wang and A. Molnar, IEEE J. Solid-State Circuits **47**, 257 (2012).
9. A. Molnar, A. Wang, and P. Gill, "Light field image sensor with an angle-sensitive pixel (ASP) device," U.S. patent 8,809,758 B2 (August19, 2014).
10. H. Chen and L. B. Wolff, Int. J. Comput. Vis. **28**, 73 (1998).
11. Y. Y. Schechner, S. G. Narasimhan, and S. K. Nayar, Appl. Opt. **42**, 511 (2003).
12. T. Charanya, T. York, S. Bloch, G. Sudlow, R. Tang, W. Akers, D. Rubin, V. Gruev, and S. Achilefu, J. Biomed. Opt. **19**, 126002 (2014).
13. J. Millerd, N. Brock, J. Hayes, M. North-Morris, M. Novak, and J. Wyant, Proc. SPIE **5531**, 304 (2004).
14. T. Tahara, K. Ito, M. Fujii, T. Kakue, Y. Shimozato, Y. Awatsuji, K. Nishio, S. Ura, T. Kubota, and O. Matoba, Opt. Express **18**, 18975 (2010).
15. Z. Zhang, F. Dong, T. Cheng, K. Qiu, Q. Zhang, W. Chu, and X. Wu, Rev. Sci. Instrum. **85**, 105002 (2014).
16. T. Onuma and Y. Otani, Opt. Commun. **315**, 69 (2014).
17. V. Gruev, R. Perkins, and T. York, Opt. Express **18**, 19087 (2010).
18. V. Gruev, A. Ortu, N. Lazarus, J. Van der Spiegel, and N. Engheta, Opt. Express **15**, 19292 (2007).
19. M. Sarkar and A. Theuwissen, *A Biologically Inspired CMOS Image Sensor* (Springer, 2013).
20. D. Beghuin, E. Cuche, P. Dahlgren, C. Depeursinge, G. Delacretaz, and R. P. Salathe, Electron. Lett. **35**, 2053 (1999).
21. T. Tahara, Y. Awatsuji, Y. Shimozato, T. Kubota, and O. Matoba, Opt. Lett. **36**, 3254 (2011).
22. M. Hirsch, S. Sivaramakrishnan, S. Jayasuriya, A. Wang, A. Molnar, R. Raskar, and G. Wetzstein, *IEEE Int. Conf. Comp. Photography* (2014), pp. 1–10.
23. S. K. Nayar, X. S. Fang, and T. Boult, IEEE Comp. Vis. Pattern Recogn. **593**, 583 (1993).
24. E. Gilboar, J. P. Cunningham, A. Nehorai, and V. Gruev, Opt. Express **22**, 15277 (2014).